2023 IEEE Symposium Series on Computational Intelligence (SSCI)
Mexico City, Mexico. December 5-8, 2023

Empirical Hypervolume Optimal μ-Distributions on Complex Pareto Fronts

Ke Shang, Tianye Shu, Guotong Wu, Yang Nan, Lie Meng Pang, Hisao Ishibuchi*
Guangdong Provincial Key Laboratory of Brain-inspired Intelligent Computation
Department of Computer Science and Engineering
Southern University of Science and Technology
Shenzhen, China

***Abstract*—Hypervolume optimal μ-distribution is the distribution of μ solutions maximizing the hypervolume indicator of μ solutions on a specific Pareto front. Most studies have focused on simple Pareto fronts such as triangular and inverted triangular Pareto fronts. There is almost no study which focuses on complex Pareto fronts such as disconnected and partially degenerate Pareto fronts. However, most real-world multi-objective optimization problems have such a complex Pareto front. Thus, it is of great practical significance to study the hypervolume optimal μ-distribution on the complex Pareto fronts. In this paper, we study this issue by empirically showing the hypervolume optimal μ-distributions on the Pareto fronts of some representative artificial and real-world test problems. Our results show that, in general, maximizing the hypervolume indicator does not lead to uniformly distributed solution sets on the complex Pareto fronts. We also give some suggestions related to the use of the hypervolume indicator for performance evaluation of evolutionary multi-objective optimization algorithms.**

***Index Terms*—Hypervolume, optimal μ-distribution, complex Pareto front, multi-objective optimization**

I. Introduction

The hypervolume indicator [1] is a well-known performance indicator in evolutionary multi-objective optimization (EMO). It has been widely-used for performance evaluation of EMO algorithms since it can evaluate their convergence and diversity performance simultaneously [2]. The ability to evaluate the convergence performance is due to its Pareto compliance property [3]. Better solution sets with respect to the Pareto dominance relation always have larger hypervolume values. The ability to evaluate the diversity performance is based on the following commonly-believed implicit assumption: A larger hypervolume value means a more diverse solution set. However, this issue is under-investigated in the EMO community.

To deeply understand the ability of the hypervolume indicator for the diversity performance evaluation, many studies have been conducted on the so-called hypervolume optimal μ-distribution. The hypervolume optimal μ-distribution research involves investigating the distribution of μ solutions maximizing the hypervolume indicator on a Pareto front. The hypervolume optimal μ-distribution can directly indicate whether optimizing the hypervolume indicator can lead to a diverse solution set or not on a Pareto front, and further provide guidance of using the hypervolume indicator for the diversity performance evaluation.

Currently, most studies on the hypervolume optimal μ-distribution have focused on the simple Pareto fronts. For example, the two-objective linear Pareto front was considered in [4], [5], [6]. The two-objective convex and concave Pareto fronts were also investigated in [5]. In the three-objective case, the linear triangular and inverted triangular Pareto fronts were studied in [7]. The triangular and inverted triangular Pareto fronts with convex and concave curvatures were also studied in [8], [9]. Some simple line-based degenerate Pareto fronts were investigated in [10], [11], [12]. All these Pareto fronts have quite simple structures. Most studies suggest that if the reference point is properly specified, a diverse solution set on the entire Pareto front can be obtained for hypervolume maximization.

However, most real-world problems have very complex Pareto fronts such as disconnected and partially degenerate Pareto fronts. Currently, there is almost no study which focuses on investigating the hypervolume optimal μ-distributions on the complex Pareto fronts. It is unclear whether a diverse solution set can be obtained or not for hypervolume maximization. Thus, it is of great practical significance to study the hypervolume optimal μ-distribution on the complex Pareto fronts. In this paper, we choose some representative complex Pareto fronts of artificial and real-world test problems, and empirically study the hypervolume optimal μ-distributions. We consider three-objective test problems in our study in order to visually show the solution distributions for hypervolume maximization on the complex Pareto fronts. Based on our experimental results, we give some suggestions related to the use of the hypervolume indicator for performance evaluation of EMO algorithms.

The remainder of this paper is organized as follows. Section II explains the foundations of the hypervolume optimal μ-distribution. Section III shows the complex Pareto fronts considered in our study. Section IV empirically investigates the

This work was supported by National Natural Science Foundation of China (Grant No. 62002152, 62250710163, 62250710682), Guangdong Provincial Key Laboratory (Grant No. 2020B121201001), the Program for Guangdong Introducing Innovative and Enterpreneurial Teams (Grant No. 2017ZT07X386), The Stable Support Plan Program of Shenzhen Natural Science Fund (Grant No. 20200925174447003), Shenzhen Science and Technology Program (Grant No. KQTD20161125143555 31).
*Corresponding author: Hisao Ishibuchi (hisao@sustech.edu.cn)

hypervolume optimal μ- distributions on some representative complex Pareto fronts. Section V further investigates the obtained hypervolume optimal u-distributions. Finally, Section VI concludes this paper.

II. Hypervolume optimal μ-distribution

A. Basic Definitions

The hypervolume indicator is the fundamental concept in our study. Formally, the hypervolume indicator is defined as follows.

Definition 1 (Hypervolume [2])**.** *Given a solution set S and a reference point $\mathbf{r} \in \mathbb{R}^m$ in the objective space, the hypervolume of S is defined as*

$$HV(S, \mathbf{r}) = \mathcal{L}\left(\bigcup_{\mathbf{s}\in S}\{\mathbf{s}'|\mathbf{s} \prec \mathbf{s}' \prec \mathbf{r}\}\right), \quad (1)$$

where $\mathcal{L}(.)$ is the Lebesgue measure of a set, and $\mathbf{s} \prec \mathbf{s}'$ denotes that $\mathbf{s}$ Pareto dominates $\mathbf{s}'$ (i.e., $s_i \leq s'_i$ for all $i = 1, ..., m$ and $s_j < s'_j$ for at least one $j = 1, ..., m$ in the minimization case, where m is the number of objectives).

Based on the definition of the hypervolume indicator, we can define the hypervolume optimal μ-distribution as follows.

Definition 2 (Hypervolume optimal μ-distribution [2])**.** *Given a Pareto front $\mathcal{F} \subset \mathbb{R}^m$ and a reference point $\mathbf{r} \in \mathbb{R}^m$, the hypervolume optimal μ-distribution is $\mu \in \mathbb{N}$ points on the Pareto front which maximize the hypervolume of μ points. The set A containing the optimal μ points is*

$$A = \arg \max_{|A'|=\mu,\ A'\subset\mathcal{F}} HV(A', \mathbf{r}). \quad (2)$$

B. Hypervolume Optimal μ-Distributions on Simple Pareto Fronts

Existing studies mainly focus on investigating the hypervolume optimal μ-distributions on simple Pareto fronts. In this subsection, we briefly review some existing results on the two-objective and three-objective linear Pareto fronts.

Without loss of generality, we assume minimization problems, and the nadir point of the Pareto front $\mathcal{F}$ is denoted as $\mathbf{nadir}$. The nadir point is the point with the worst value for each objective. For hypervolume calculation, the reference point $\mathbf{r}$ is specified as

$$\mathbf{r} = \alpha \times \mathbf{nadir}, \quad (3)$$

where α is a parameter. Usually $\alpha \geq 1$.

For the two-objective minimization case, it has been proved that the μ solutions are equispaced on the linear Pareto front for hypervolume maximization [5]. Fig. 1 illustrates the hypervolume optimal μ-distributions on the two-objective linear Pareto front with different reference point specifications. If $\alpha \geq 1 + \frac{1}{\mu-1}$, the two extreme points of the Pareto front are included in the hypervolume optimal μ-distribution, and the location of the reference point does not influence the hypervolume optimal μ-distribution [6].

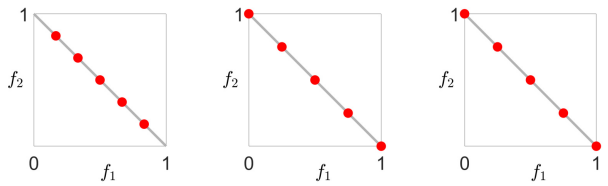

(a) $\alpha = 1$ (b) $\alpha = 1.25$ (c) $\alpha = 100$

Fig. 1. Hypervolume optimal μ-distributions ($\mu = 5$) with different reference point specifications on the two-objective linear Pareto front.

For the three-objective minimization case, the hypervolume optimal μ-distributions on the linear triangular and inverted triangular Pareto fronts have been empirically investigated in [7]. It has been shown that the μ solutions are uniformly distributed on both types of Pareto fronts for hypervolume maximization when the reference point is specified as

$$\alpha = 1 + \frac{1}{H}, \quad (4)$$

where H is an integer satisfying $C_{m-1}^{H+m-1} \leq \mu < C_{m-1}^{H+m}$, m is the number of objectives, and C_b^a is the total number of combinations for choosing b elements from a set of a elements. Furthermore, if $\alpha > 1 + \frac{1}{H}$, the location of the reference point does not influence the hypervolume optimal μ-distribution on the triangular Pareto front whereas it significantly influences the hypervolume optimal μ-distribution on the inverted triangular Pareto front. When the reference point is sufficiently far, all solutions are distributed on the boundary of the linear inverted triangular Pareto front. Fig. 2 illustrates the empirical hypervolume optimal μ-distributions obtained by SMS-EMOA [13] on the three-objective linear triangular and inverted triangular Pareto fronts with different reference point specifications.

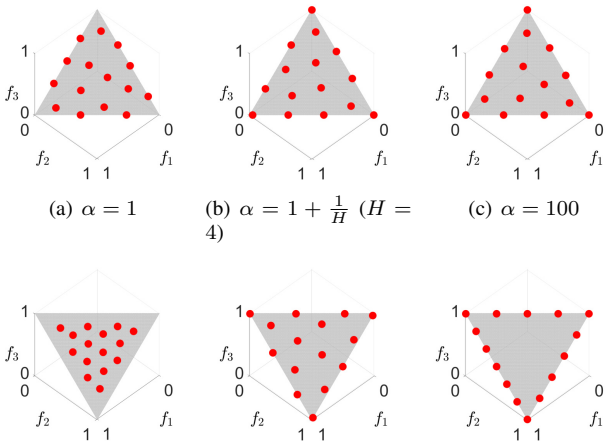

(a) $\alpha = 1$ (b) $\alpha = 1 + \frac{1}{H}$ ($H = 4$) (c) $\alpha = 100$

(d) $\alpha = 1$ (e) $\alpha = 1 + \frac{1}{H}$ ($H = 4$) (f) $\alpha = 100$

Fig. 2. Empirical hypervolume optimal μ-distributions ($\mu = 15$) with different reference point specifications obtained by SMS-EMOA on the three-objective linear triangular and inverted triangular Pareto fronts.

III. Complex Pareto fronts

In this section, we introduce the complex Pareto fronts considered in our study. We choose two sets of complex Pareto fronts: Pareto fronts of artificial test problems and Pareto fronts of real-world test problems. These two sets of Pareto fronts are explained in the following subsections.

A. Pareto Fronts of Artificial Test Problems

The first set of complex Pareto fronts are from artificial test problems. We choose three-objective DTLZ7 [14], three-objective WFG3 [15], and IMOP5-8 [16] in our study. Thus, we have six artificial test problems in total. All these test problems are available in PlatEMO[1] [17]. Their Pareto fronts are also provided in PlatEMO. Fig. 3 shows the Pareto fronts of these artificial test problems.

It should be noted that the Pareto front of WFG3 provided in PlatEMO is not correct. WFG3 was intended to have a degenerate Pareto front and this degenerate Pareto front is provided in PlatEMO. However, WFG3 actually has a mixed Pareto front with a degenerate part and a non-degenerate part [18]. We use the method in [18] to generate an approximated Pareto front for WFG3 in our study.

The characteristics of each Pareto front in Fig. 3 is described as follows. The Pareto front of DTLZ7 has four disconnected parts. The Pareto front of WFG3 is the combination of a degenerate part and a non-degenerate part [18]. The Pareto front of IMOP5 consists of eight circles. The Pareto front of IMOP6 has nine square holes in the square Pareto front. The Pareto front of IMOP7 is a part of a unit sphere in the first octant. The Pareto front of IMOP8 contains 100 disconnected subregions and each subregion contains infinite points [16].

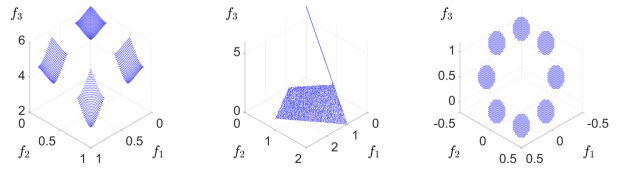

(a) DTLZ7 (b) WFG3 (c) IMOP5

(d) IMOP6 (e) IMOP7 (f) IMOP8

Fig. 3. Pareto fronts of artificial test problems.

B. Pareto Fronts of Real-world Test Problems

The second set of complex Pareto fronts are from real-world test problems. In our study, we choose six problems from the RE test suite[2] [19]: two bar truss design (RE3-3-1), welded beam design (RE3-4-2), disc brake design (RE3-4-3), vehicle crashworthiness design (RE3-5-4), speed reducer design (RE3-7-5), and rocket injector design (RE3-4-7). Different from the artificial test problems, the true Pareto fronts of these real-world test problems are usually unknown. The authors of the RE test suite have provided the approximated Pareto fronts of these real-world test problems. We have also verified the provided approximated Pareto fronts by running different EMO algorithms on these problems. We directly use the provided approximated Pareto fronts in our study. Fig. 4 shows the approximated Pareto fronts of these real-world test problems.

The characteristics of each Pareto front in Fig. 4 is described as follows. The Pareto front of RE3-3-1 has two parts: one part is almost parallel to the $f_1 - f_3$ plane, and the other part is almost parallel to the $f_2 - f_3$ plane. The Pareto front of RE3-4-2 is a degenerate Pareto front with two parts: one part is almost parallel to the f_1 axis, and the other part is almost parallel to the $f_2 - f_3$ plane. The Pareto front of RE3-4-3 is a mixed Pareto front with a degenerate part and a non-degenerate part: the degenerate part is almost parallel to the f_3 axis, and the non-degenerate part is almost parallel to the $f_1 - f_2$ plane. The Pareto front of RE3-5-4 has four disconnected parts. The Pareto front of RE3-7-5 has three parts: the first part is almost parallel to the f_1 axis, the second part is almost parallel to the $f_1 - f_2$ plane, and the third part is almost parallel to the $f_2 - f_3$ plane. The Pareto front of RE3-4-7 has a complex and irregular shape.

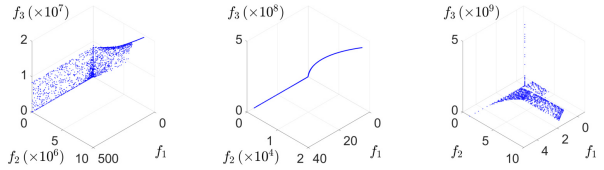

(a) RE3-3-1 (b) RE3-4-2 (c) RE3-4-3

(d) RE3-5-4 (e) RE3-7-5 (f) RE3-4-7

Fig. 4. Pareto fronts of real-world problems [19].

IV. Empirical hypervolume optimal μ-distributions

Theoretic analysis of the hypervolume optimal μ-distributions on the complex Pareto fronts is not an easy task [20]. Instead, we conduct empirical investigations as in [7], [9] in our study. An approximated optimal μ-distribution is obtained by running a search algorithm on each problem. In this section, the search algorithm, the settings, and the obtained distributions are presented. We use a large amount

[1]https://github.com/BIMK/PlatEMO

[2]https://github.com/ryojitanabe/reproblems

of computation time to optimize the distribution as much as possible. In the next section, we show that the obtained distribution is actually very close to the hypervolume optimal μ-distributions whereas some of them are counterintuitive.

A. Search Algorithm

To search for the hypervolume optimal μ-distributions on the complex Pareto fronts, we use the combination of NSGA-II [21] and SMS-EMOA [13] as the search algorithm. The basic idea of the search algorithm is to use NSGA-II for the first-half of the function evaluations and SMS-EMOA for the second-half of the function evaluations. NSGA-II is used for the first-half of the function evaluations since NSGA-II can quickly push the population to the Pareto front and maintain a diversified solution set on the Pareto front. Then SMS-EMOA is used for the second-half of the function evaluations since SMS-EMOA is able to refine the distribution of solutions on the Pareto front for hypervolume maximization.

In SMS-EMOA, we fix the reference point based on the nadir point of the true Pareto front (the approximated Pareto front in the case of real-world problems) in order to search for the hypervolume optimal μ-distribution on the entire Pareto front. The reference point is specified as in Eq. (3).

B. Settings

To make sure that the obtained solution set by the search algorithm is optimal or close-to-optimal for hypervolume maximization, we set the maximum number of function evaluations as 100,000. The population size (i.e., μ) is set as 100. For each test problem, the search algorithm is run 100 times independently and the best solution set among 100 solution sets (i.e., the one with the maximum hypervolume value) is presented as the empirical hypervolume optimal μ-distribution.

For the reference point specification in SMS-EMOA, we examine two settings: $\alpha = 1 + \frac{1}{H}$ ($H = 12$ for $\mu = 100$) and $\alpha = 100$. We examine $\alpha = 1 + \frac{1}{H}$ since it is the suggested reference point specification in [22], which can lead to uniformly distributed solution sets on the linear triangular and inverted triangular Pareto fronts as shown in Section II-B. In addition, we examine $\alpha = 100$ to check whether the location of the reference point influences the hypervolume optimal μ-distributions or not on the complex Pareto fronts.

C. Results

Figs. 5-8 show the obtained empirical hypervolume optimal μ-distributions on the complex Pareto fronts of the considered artificial and real-world problems.

For the Pareto fronts of the artificial test problems, when $\alpha = 1 + \frac{1}{H}$ in Fig. 5, uniform solution sets cannot always be obtained. Only for IMOP6 and IMOP8, relatively uniform solution sets are obtained. For other problems, non-uniform solution sets are obtained. For example, for DTLZ7, many solutions are densely distributed on the top three parts of the Pareto front. For WFG3, solutions are more densely distributed on the degenerate part of the Pareto front. For IMOP5, most solutions are distributed on the boundaries of the eight circles. For IMOP7, most solutions are distributed on the boundaries of the Pareto front.

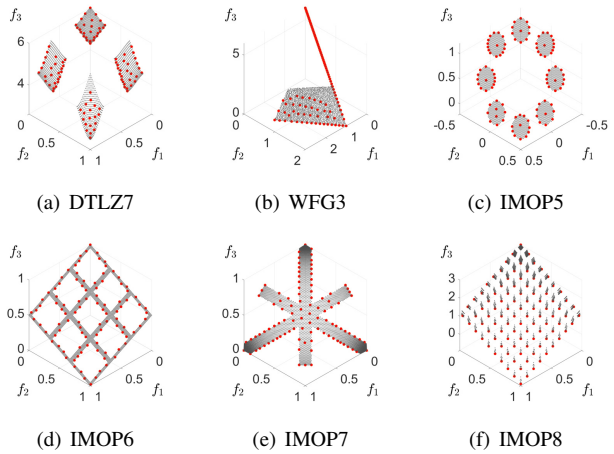

(a) DTLZ7 (b) WFG3 (c) IMOP5

(d) IMOP6 (e) IMOP7 (f) IMOP8

Fig. 5. Empirical hypervolume optimal μ-distributions ($\mu = 100$) on the Pareto fronts of artificial test problems with $\alpha = 1 + \frac{1}{H}$ ($H = 12$).

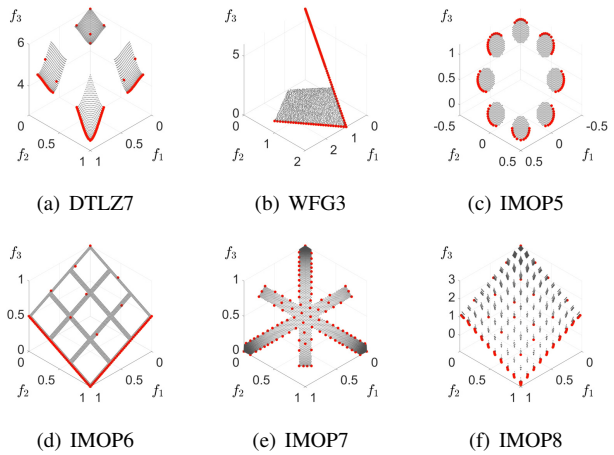

(a) DTLZ7 (b) WFG3 (c) IMOP5

(d) IMOP6 (e) IMOP7 (f) IMOP8

Fig. 6. Empirical hypervolume optimal μ-distributions ($\mu = 100$) on the Pareto fronts of artificial test problems with $\alpha = 100$.

When $\alpha = 100$ in Fig. 6, most distributions change dramatically. Only for IMOP7, the solution distribution has almost no change. This is because the Pareto front shape of IMOP7 is generally triangular. After the three extreme solutions $(0, 0, 1)$, $(0, 1, 0)$, and $(1, 0, 0)$ are obtained, the hypervolume contributions of all other solutions cannot be affected by the location of the reference point. For other problems, most solutions tend to distribute on some specific boundaries of the Pareto front. For DTLZ7, IMOP6, and IMOP8, most solutions are distributed on the lower boundaries of the Pareto fronts, which have an inverted triangular shape. This observation is consistent with the reported results that the location of the reference point has a large effect on the solutions distributed on the inverted triangular boundaries of the Pareto front as shown in Section II-B. For WFG3 and IMOP5, solutions tend to distribute on the outside boundaries of the Pareto front.

For the Pareto fronts of real-world problems, when $\alpha = 1 + \frac{1}{H}$ in Fig. 7, uniform solution sets cannot be obtained for any problem. For RE3-3-1, RE3-4-2, and RE3-4-3, solutions only distribute on a small part of the Pareto front. This is because for these test problems, the Pareto fronts contain many dominance resistant solutions (DRS) [23], [24], which have very small (almost zero) hypervolume contributions. Thus, these DRSs are not included in the hypervolume optimal μ-distributions. For RE3-5-4, RE3-7-5, and RE3-4-7, although a wider solution set is obtained on the Pareto front, some part of the Pareto front are not covered by the obtained solution set.

When $\alpha = 100$ in Fig. 8, most distributions have no dramatic change from Fig. 7 except for RE3-5-4 and RE3-4-7. For example, for RE3-3-1, RE3-4-2, RE3-4-3, and RE3-7-5, the visual difference between Fig. 7 and Fig. 8 is minor. This is because all these Pareto fronts contain many DRSs. DRSs usually have small hypervolume contributions even when the reference point is very far. Thus, the hypervolume optimal μ-distributions on these Pareto fronts are insensitive to the location of the reference point. For RE3-5-4 and RE3-4-7, most solutions tend to distribute on the outside boundaries of the Pareto fronts. This shows that the hypervolume optimal μ-distributions on these Pareto fronts are sensitive to the location of the reference point.

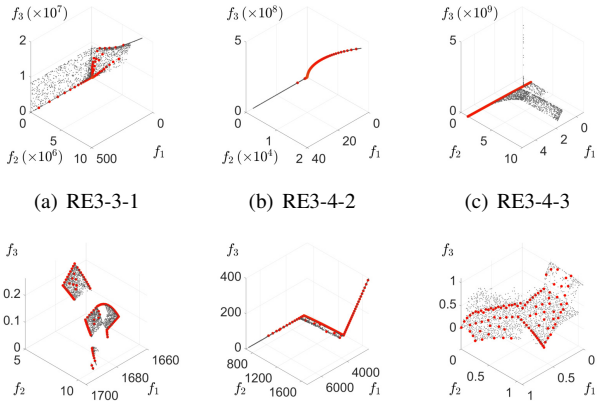

(a) RE3-3-1 (b) RE3-4-2 (c) RE3-4-3

(d) RE3-5-4 (e) RE3-7-5 (f) RE3-4-7

Fig. 7. Empirical hypervolume optimal μ-distributions ($\mu = 100$) on the Pareto fronts of real-world problems with $\alpha = 1 + \frac{1}{H}$ ($H = 12$).

V. Further Investigations

A. Compare with Other Algorithms

In Section IV, we run our search algorithm on each problem many times to obtain the empirical hypervolume optimal μ-distribution. To further examine the reliability of the obtained solution set (i.e., its optimality), we compare each solution set obtained in Section IV with the solution sets obtained by a greedy hypervolume subset selection (GHSS) algorithm [25] and a distance-based subset selection (DSS) algorithm [26]. Both GHSS and DSS are greedy subset selection algorithms. GHSS selects a subset with the objective of maximizing the hypervolume value of the selected subset. It has been theoretically proved that the subset selected by GHSS has at least $(1 - 1/e)$ times the hypervolume value of the optimal subset [27]. DSS selects a subset with the objective of maximizing the uniformity level[3] of the selected subset [29]. DSS aims to select a uniform solution set on the entire Pareto front.

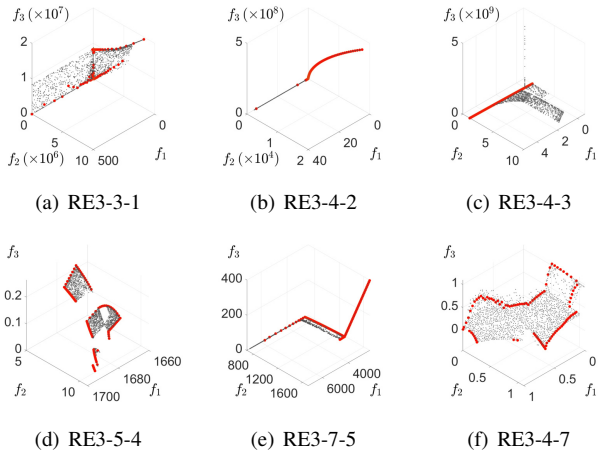

(a) RE3-3-1 (b) RE3-4-2 (c) RE3-4-3

(d) RE3-5-4 (e) RE3-7-5 (f) RE3-4-7

Fig. 8. Empirical hypervolume optimal μ-distributions ($\mu = 100$) on the Pareto fronts of real-world problems with $\alpha = 100$.

We use GHSS and DSS algorithms to select μ solutions from a candidate solution set on the Pareto front. For the Pareto fronts of the artificial test problems, we generate the candidate solution sets by uniformly sampling solutions on the Pareto fronts. This can be done directly in PlatEMO. The number of solutions in each candidate solution set is about 2000. For the Pareto fronts of the real-world problems, we directly use the approximated Pareto fronts as the candidate solution sets. We set $\alpha = 1 + \frac{1}{H}$, then we compare the normalized hypervolume values of the solution sets obtained by the three algorithms. Experimental results are summarized in Table I. To calculate the normalized hypervolume value of a solution set, we first normalize the solution set based on the ideal and nadir points of the Pareto front so that these two points are $(0, 0, 0)$ and $(1, 1, 1)$ respectively, then we set the reference point for the hypervolume indicator as (α, α, α).

From Table I, we can see that the solution sets obtained by the search algorithm always have the highest hypervolume values compared with GHSS and DSS. This shows the reliability of the solution sets obtained by the search algorithm as the empirical hypervolume optimal μ-distributions (in the sense that they are always better than the solution sets obtained by the greedy algorithm). The solution sets obtained by DSS always have the lowest hypervolume values. This means that uniform solution sets on these complex Pareto fronts cannot be evaluated as good solution sets based on the hypervolume indicator.

We further compare the solution sets obtained by the three algorithms on the six real-world Pareto fronts in Fig. 9. We

[3]The uniformity level of a set is the minimum distance value between any two solutions in this set [28].

TABLE I

THE NORMALIZED HYPERVOLUME VALUES OF THE SOLUTION SETS OBTAINED BY THE SEARCH ALGORITHM, GHSS, AND DSS WITH $\alpha = 1 + \frac{1}{H}$ ($H = 12$). THE HIGHEST HYPERVOLUME VALUE IN EACH ROW IS HIGHLIGHTED IN BOLD.

Problems	Search Algorithm	GHSS	DSS
DTLZ7	**0.3413844**	0.3406833	0.3369402
WFG3	**0.6831202**	0.6823060	0.6651156
IMOP5	**0.6209844**	0.6177635	0.6079791
IMOP6	**0.6624239**	0.6600987	0.6560942
IMOP7	**0.6541685**	0.6519038	0.6451827
IMOP8	**0.6772725**	0.6725810	0.6557023
RE3-3-1	**1.2714108**	1.2714106	1.2695393
RE3-4-2	**1.2706937**	1.2706881	1.2704836
RE3-4-3	**1.1096155**	1.1084568	1.1068151
RE3-5-4	**0.0415125**	0.0414740	0.0412420
RE3-7-5	**0.5390541**	0.5390317	0.5382311
RE3-4-7	**0.8296859**	0.8277044	0.8164381

can see that the solution sets obtained by the search algorithm and GHSS are similar since both of them aim to maximize the hypervolume of the selected solution set. The solution sets obtained by DSS are more uniformly distributed over the entire Pareto fronts. However, as indicated in Table I, these solution sets have the lowest hypervolume values. The visual comparison results in Fig. 9 clearly show that uniform solution sets on the complex Pareto fronts can be evaluated as worse solution sets than nonuniform solution sets based on the hypervolume indicator.

B. Examine the Uncovered Solutions of the Pareto Front

As shown in Section IV, for most real-world test problems, the hypervolume optimal μ-distributions do not cover the entire complex Pareto fronts. Even when the reference point is very far (i.e., $\alpha = 100$), some boundary regions are not included in the optimal distributions (whereas their inside regions are included), which is quite different from the simple Pareto fronts (e.g., the linear inverted triangular Pareto front in Section II-B).

For example, for RE3-4-7 in Fig. 8, no solutions in some boundary regions are included in the obtained solution set whereas many solutions inside those regions are obtained as clearly shown in Fig. 10 (a). There are two possible reasons:

1) The search algorithm cannot find these boundary solutions. That is, these boundary solutions are very difficult to find.
2) The search algorithm can find these boundary solutions. However, these boundary solutions have very small hypervolume contributions. Thus, they are always removed by the environmental selection of SMS-EMOA.

To verify the above two possible reasons, we simulate the environmental selection in SMS-EMOA by adding one uncovered solution (i.e., the black point in Fig. 10 (a)) to the red point set (i.e., the hypervolume optimal μ-distribution obtained by the search algorithm). If the uncovered solution is always removed by SMS-EMOA, this means that the red point set is optimal or local optimal for the $(\mu + 1)$-selection

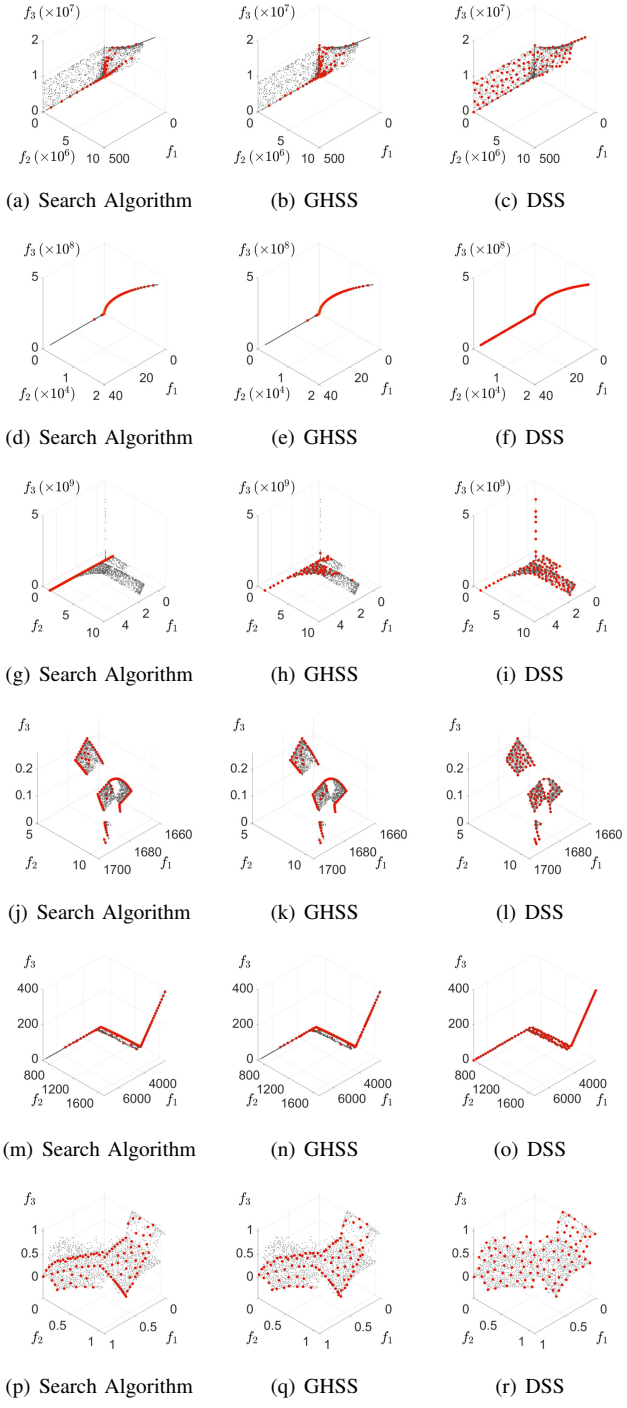

(a) Search Algorithm (b) GHSS (c) DSS

(d) Search Algorithm (e) GHSS (f) DSS

(g) Search Algorithm (h) GHSS (i) DSS

(j) Search Algorithm (k) GHSS (l) DSS

(m) Search Algorithm (n) GHSS (o) DSS

(p) Search Algorithm (q) GHSS (r) DSS

Fig. 9. Solution sets obtained by the search algorithm, GHSS, and DSS with $\alpha = 1 + \frac{1}{H}$ ($H = 12$) on the Pareto fronts of six real-world problems. Their corresponding hypervolume values are shown in Table I.

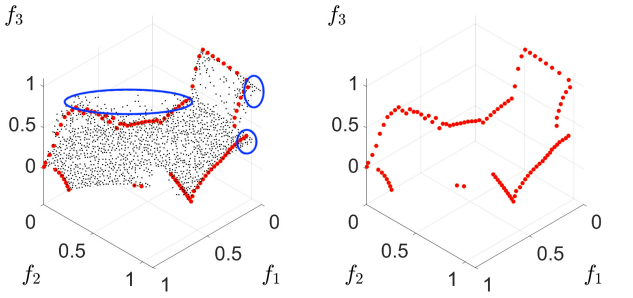

(a) The uncovered regions

(b) Simulation result of SMS-EMOA

Fig. 10. (a) Empirical optimal μ-distribution (red point set) and other solutions (black points) on the Pareto front of RE3-4-7 with $\alpha = 100$. Each blue ellipse indicates an uncovered boundary region. (b) Further examination results of each point using SMS-EMOA with $\alpha = 100$. Each black point is added to the red point set. If the black point is removed by SMS-EMOA, this point is also removed from the figure.

strategy in SMS-EMOA (i.e., the second possible reason is valid).

Fig. 10 (b) shows the simulation result. If one uncovered solution is added to the red point set and removed by SMS-EMOA, this solution is also removed in Fig. 10 (b). We can see from Fig. 10 (a) that all the uncovered solutions (i.e., black points in Fig. 10 (a)) are removed by SMS-EMOA. This verifies the second possible reason, and further shows the high reliability of the obtained hypervolume optimal μ-distribution (i.e., its high optimality).

The reason for the uncovered boundaries in Fig. 10 (a) is that these solutions are DRSs. So these solutions have very small (almost zero) hypervolume contributions even when the reference point is very far. Therefore, they are not included in the hypervolume optimal μ-distribution.

VI. Conclusions

In this paper, we empirically investigated the hypervolume optimal μ-distributions on some complex Pareto fronts of artificial and real-world test problems. The main observation is that, in general, maximizing the hypervolume indicator does not lead to a uniform solution set on a complex Pareto front. Thus, it is very likely that a uniform solution set on a complex Pareto front is evaluated as a bad solution set based on the hypervolume indicator. Currently, many EMO algorithms are designed to obtain a uniform solution set on the entire Pareto front. Thus, we have the following three suggestions about the use of the hypervolume indicator for performance evaluation of EMO algorithms.

1) It is suggested to use the hypervolume indicator for performance evaluation if the algorithms to be evaluated are designed for hypervolume maximization (e.g., SMS-EMOA [13], HypE [30], FV-MOEA [31], and R2HCA-EMOA [32]). Since these algorithms aim to maximize the hypervolume value of the population, using the hypervolume indicator to evaluate their performance is the most suitable choice.
2) It is not suggested to use the hypervolume indicator for performance evaluation if the algorithms to be evaluated are designed for obtaining a uniform solution set on the Pareto front, especially for real-world problems. This is because real-world problems usually have complex Pareto fronts. Using the hypervolume indicator for performance evaluation may give us misleading conclusions. Instead, other indicators such as IGD [33] and uniformity level [28] are better choices.
3) When different algorithms are compared, it is advisable to use multiple indicators including the hypervolume and IGD (or uniformity level) indicators. If clearly different evaluation results are obtained from a test problem, those results suggest that uniform distributions are not good for the hypervolume indicator. That is, the Pareto front shape of the test problem can be complicated. In this case, comparison of different algorithms may depend on the preference of the decision maker about the solution distribution.

In the future, we will consider more real-world test problems and examine the corresponding hypervolume optimal μ-distributions. We will also consider problems with more than three objectives. It is not easy to visually examine the solution distributions in a high-dimensional objective space with more than three objectives. Thus, some other methods may be needed to analyze the solution distributions, which is an interesting future research direction. Our experimental results show the difficulty of solution set evaluations. For example, in Fig. 9, well-distributed solution sets over the entire Pareto fronts have the smallest hypervolume values. We may need decision maker's preference about the distribution of solutions to further compare different solution sets. This is also an interesting future research direction.

References

[1] E. Zitzler, L. Thiele, M. Laumanns, C. M. Fonseca, and V. G. Da Fonseca, "Performance assessment of multiobjective optimizers: An analysis and review," *IEEE Transactions on Evolutionary Computation*, vol. 7, no. 2, pp. 117–132, 2003.

[2] K. Shang, H. Ishibuchi, L. He, and L. M. Pang, "A survey on the hypervolume indicator in evolutionary multiobjective optimization," *IEEE Transactions on Evolutionary Computation*, vol. 25, no. 1, pp. 1–20, 2021.

[3] E. Zitzler, D. Brockhoff, and L. Thiele, "The hypervolume indicator revisited: On the design of pareto-compliant indicators via weighted integration," in *Evolutionary Multi-Criterion Optimization: 4th International Conference, EMO 2007, Matsushima, Japan, March 5-8, 2007. Proceedings 4*. Springer, 2007, pp. 862–876.

[4] M. Emmerich, A. Deutz, and N. Beume, "Gradient-based/evolutionary relay hybrid for computing pareto front approximations maximizing the s-metric," in *Hybrid Metaheuristics: 4th International Workshop, HM 2007, Dortmund, Germany, October 8-9, 2007. Proceedings 4*. Springer, 2007, pp. 140–156.

[5] A. Auger, J. Bader, D. Brockhoff, and E. Zitzler, "Theory of the hypervolume indicator: optimal μ-distributions and the choice of the reference point," in *Proceedings of the Tenth ACM SIGEVO Workshop on Foundations of Genetic Algorithms*, 2009, pp. 87–102.

[6] D. Brockhoff, "Optimal μ-distributions for the hypervolume indicator for problems with linear bi-objective fronts: Exact and exhaustive results," in *Simulated Evolution and Learning: 8th International Conference, SEAL 2010, Kanpur, India, December 1-4, 2010. Proceedings 8*. Springer, 2010, pp. 24–34.

[7] H. Ishibuchi, R. Imada, Y. Setoguchi, and Y. Nojima, "Hypervolume subset selection for triangular and inverted triangular pareto fronts of three-objective problems," in *Proceedings of the 14th ACM/SIGEVO Conference on Foundations of Genetic Algorithms*, 2017, pp. 95–110.

[8] ——, "How to specify a reference point in hypervolume calculation for fair performance comparison," *Evolutionary Computation*, vol. 26, no. 3, pp. 411–440, 2018.

[9] H. Ishibuchi, R. Imada, N. Masuyama, and Y. Nojima, "Comparison of hypervolume, igd and igd+ from the viewpoint of optimal distributions of solutions," in *Evolutionary Multi-Criterion Optimization: 10th International Conference, EMO 2019, East Lansing, MI, USA, March 10-13, 2019, Proceedings 10*. Springer, 2019, pp. 332–345.

[10] P. K. Shukla, N. Doll, and H. Schmeck, "A theoretical analysis of volume based pareto front approximations," in *Proceedings of the 2014 annual conference on genetic and evolutionary computation*, 2014, pp. 1415–1422.

[11] K. Shang, H. Ishibuchi, W. Chen, and L. Adam, "Hypervolume optimal-distributions on line-based pareto fronts in three dimensions," in *Parallel Problem Solving from Nature–PPSN XVI: 16th International Conference, PPSN 2020, Leiden, The Netherlands, September 5-9, 2020, Proceedings, Part II*. Springer, 2020, pp. 257–270.

[12] K. Shang, H. Ishibuchi, W. Chen, Y. Nan, and W. Liao, "Hypervolume-optimal μ-distributions on line/plane-based pareto fronts in three dimensions," *IEEE Transactions on Evolutionary Computation*, vol. 26, no. 2, pp. 349–363, 2022.

[13] N. Beume, B. Naujoks, and M. Emmerich, "Sms-emoa: Multiobjective selection based on dominated hypervolume," *European Journal of Operational Research*, vol. 181, no. 3, pp. 1653–1669, 2007.

[14] K. Deb, L. Thiele, M. Laumanns, and E. Zitzler, *Scalable test problems for evolutionary multiobjective optimization*. Springer London, 2005.

[15] S. Huband, P. Hingston, L. Barone, and L. While, "A review of multiobjective test problems and a scalable test problem toolkit," *IEEE Transactions on Evolutionary Computation*, vol. 10, no. 5, pp. 477–506, 2006.

[16] Y. Tian, R. Cheng, X. Zhang, M. Li, and Y. Jin, "Diversity assessment of multi-objective evolutionary algorithms: Performance metric and benchmark problems [research frontier]," *IEEE Computational Intelligence Magazine*, vol. 14, no. 3, pp. 61–74, 2019.

[17] Y. Tian, R. Cheng, X. Zhang, and Y. Jin, "Platemo: A matlab platform for evolutionary multi-objective optimization [educational forum]," *IEEE Computational Intelligence Magazine*, vol. 12, no. 4, pp. 73–87, 2017.

[18] H. Ishibuchi, H. Masuda, and Y. Nojima, "Pareto fronts of many-objective degenerate test problems," *IEEE Transactions on Evolutionary Computation*, vol. 20, no. 5, pp. 807–813, 2016.

[19] R. Tanabe and H. Ishibuchi, "An easy-to-use real-world multi-objective optimization problem suite," *Applied Soft Computing*, vol. 89, p. 106078, 2020.

[20] A. Auger, J. Bader, and D. Brockhoff, "Theoretically investigating optimal μ-distributions for the hypervolume indicator: First results for three objectives," in *Parallel Problem Solving from Nature, PPSN XI: 11th International Conference, Kraków, Poland, September 11-15, 2010, Proceedings, Part I 11*. Springer, 2010, pp. 586–596.

[21] K. Deb, A. Pratap, S. Agarwal, and T. Meyarivan, "A fast and elitist multiobjective genetic algorithm: Nsga-ii," *IEEE Transactions on Evolutionary Computation*, vol. 6, no. 2, pp. 182–197, 2002.

[22] H. Ishibuchi, R. Imada, Y. Setoguchi, and Y. Nojima, "Reference point specification in hypervolume calculation for fair comparison and efficient search," in *Proceedings of the Genetic and Evolutionary Computation Conference*, 2017, pp. 585–592.

[23] Z. Wang, Y.-S. Ong, and H. Ishibuchi, "On scalable multiobjective test problems with hardly dominated boundaries," *IEEE Transactions on Evolutionary Computation*, vol. 23, no. 2, pp. 217–231, 2019.

[24] H. Ishibuchi, T. Matsumoto, N. Masuyama, and Y. Nojima, "Effects of dominance resistant solutions on the performance of evolutionary multi-objective and many-objective algorithms," in *Proceedings of the 2020 Genetic and Evolutionary Computation Conference*, 2020, pp. 507–515.

[25] A. P. Guerreiro, C. M. Fonseca, and L. Paquete, "Greedy hypervolume subset selection in low dimensions," *Evolutionary Computation*, vol. 24, no. 3, pp. 521–544, 2016.

[26] H. K. Singh, K. S. Bhattacharjee, and T. Ray, "Distance-based subset selection for benchmarking in evolutionary multi/many-objective optimization," *IEEE Transactions on Evolutionary Computation*, vol. 23, no. 5, pp. 904–912, 2019.

[27] G. L. Nemhauser, L. A. Wolsey, and M. L. Fisher, "An analysis of approximations for maximizing submodular set functions—i," *Mathematical Programming*, vol. 14, pp. 265–294, 1978.

[28] S. Sayın, "Measuring the quality of discrete representations of efficient sets in multiple objective mathematical programming," *Mathematical Programming*, vol. 87, pp. 543–560, 2000.

[29] K. Shang, H. Ishibuchi, and Y. Nan, "Distance-based subset selection revisited," in *Proceedings of the Genetic and Evolutionary Computation Conference*, 2021, pp. 439–447.

[30] J. Bader and E. Zitzler, "Hype: An algorithm for fast hypervolume-based many-objective optimization," *Evolutionary computation*, vol. 19, no. 1, pp. 45–76, 2011.

[31] S. Jiang, J. Zhang, Y.-S. Ong, A. N. Zhang, and P. S. Tan, "A simple and fast hypervolume indicator-based multiobjective evolutionary algorithm," *IEEE Transactions on Cybernetics*, vol. 45, no. 10, pp. 2202–2213, 2015.

[32] K. Shang and H. Ishibuchi, "A new hypervolume-based evolutionary algorithm for many-objective optimization," *IEEE Transactions on Evolutionary Computation*, vol. 24, no. 5, pp. 839–852, 2020.

[33] C. A. Coello Coello and M. Reyes Sierra, "A study of the parallelization of a coevolutionary multi-objective evolutionary algorithm," in *MICAI 2004: Advances in Artificial Intelligence: Third Mexican International Conference on Artificial Intelligence, Mexico City, Mexico, April 26-30, 2004. Proceedings 3*. Springer, 2004, pp. 688–697.